Some Properties of T-Septum Waveguides

YANG ZHANG AND WILLIAM T. JOINES, MEMBER, IEEE

Abstract — **Equations and curves giving cutoff frequency and impedance are presented for rectangular waveguide having a T-septum on one or both sides. It is shown that the T-septum waveguide has a lower cutoff frequency and wider bandwidth than a ridged waveguide of the same gap parameters. The impedance characteristic is shown to be almost the same as that of the ridged guide. Equations and charts are presented to facilitate the design of T-septum waveguides. Experimental measurements show a good agreement with the theoretical predictions. The theoretical results are obtained by the formulation of an integral eigenvalue equation which is subsequently solved numerically by application of the Ritz–Galerkin method. The eigenvalue spectrum is also discussed.**

I. Introduction

RIDGED WAVEGUIDES have been investigated for many years. Conclusions are that placing ridges inside a rectangular guide can greatly increase both the cutoff wavelength and the bandwidth of the dominant mode [1]–[4]. These features can be further improved by dielectric loading [5] or by adding more ridges in the guide [6].

A significant improvement in the ridged waveguide can be obtained by changing the shape of the ridge into a T-shaped septum. This was suggested by Mazumder and Saha [7], [8] in their preliminary analysis of a double T-septum waveguide, which showed a decrease in the cutoff frequency of the dominant mode. Our more extensive analysis of the T-septum waveguide predicts a much greater bandwidth than that obtained by Mazumder and Saha. It appears that they have used an incorrect eigenvalue for the second lowest mode. The calculated results presented herein are verified by experimental measurements on a T-septum waveguide constructed in accordance with our design equations. The difference between theory and experiment is less than 10 percent and is well within the limits of experimental error.

To facilitate a more complete study of the T-septum waveguide, this paper formulates an integral eigenvalue problem. The homogeneous equations are solved numerically by the Ritz–Galerkin method [9]–[11] to yield a generalized matrix eigenvalue problem. The generalized eigenvalue problem is solved by applying a solution developed by Barlow and Jones [12]. The analysis presented in this paper will be restricted to TE_{10} and TE_{20} modes. The result of this investigation is a complete set of equations and charts, with which one can design any waveguide of this form. It is hoped that this design ability will lead to new application of these waveguides, and to the investigation of other shapes and forms.

Manuscript received January 20, 1987; revised April 9, 1987.

The authors are with the Department of Electrical Engineering, Duke University, Durham, NC 27706.

IEEE Log Number 8715417.

II. Formulation of Integral Eigenvalue Equation

The geometry of the T-septum waveguide is illustrated in Fig. 1. As is often the case, two symmetrical T-septa are assumed for the double T-septum guide. This symmetrical system may be analyzed in the same way as the single T-septum guide by considering one of the half-sections formed by introducing a conducting plane, as shown in Fig. 1(a). The aspect ratio of the half-section is $b/2a$. With this taken into consideration, we proceed with our analysis of the single T-septum guide. The results are easily applied to the symmetrical double T-septum guide (DTSG).

The single T-septum guide (STSG) and the coordinates used in our analysis are illustrated in Fig. 1(b). The TE modes of the fields are derivable from the Hertzian potential [13] of the form

$$\Pi_h = \boldsymbol{a}_z \frac{g(x,y)}{j\omega\mu} e^{-\gamma z} \tag{1}$$

where $g(x, y)$ is an unknown function to be determined. The scalar function $g(x, y)$ satisfies the wave equation

$$\nabla_t^2 g(x,y) + k_c^2 g(x,y) = 0 \tag{2}$$

where k_c is a waveguide eigenvalue and the propagation constant γ is given by

$$\gamma = \begin{cases} j\sqrt{k^2 - k_c^2} & k > k_c \\ \sqrt{k_c^2 - k^2} & k < k_c \end{cases} \tag{3}$$

where $j = \sqrt{-1}$ and $k = \omega\sqrt{\mu\epsilon}$. The scalar potential function is related to the electric and magnetic fields by the equations

$$\boldsymbol{E} = e^{-\gamma z}\boldsymbol{a}_z \times \nabla_t g(x,y) \tag{4a}$$

$$\boldsymbol{H} = -\frac{\gamma}{j\omega\mu} e^{-\gamma z}\nabla_t g(x,y) + \frac{k_c^2}{j\omega\mu} g(x,y) e^{-\gamma z}\boldsymbol{a}_z. \tag{4b}$$

We are interested only in the transverse components of the fields, and therefore we may define the basis fields via

$$\boldsymbol{e}_t = \boldsymbol{a}_z \times \nabla_t g(x,y) \tag{5a}$$

$$\boldsymbol{h}_t = -Y_h \boldsymbol{e}_t \times \boldsymbol{a}_z \tag{5b}$$

where $Z_h = 1/Y_h = \gamma/j\omega\mu$ is defined as the wave impedance of the guide.

0018-9480/87/0800-0769$01.00

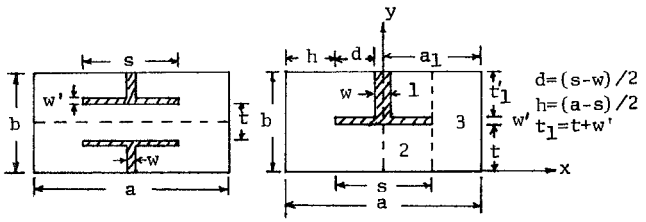

Fig. 1. Geometry of (a) double T-septum guide and (b) single T-septum guide.

The boundary conditions (BC's) require that the tangential electric field and normal magnetic field vanish on the conductors, or, equivalently, that $\boldsymbol{n}\cdot\nabla_t g(x, y) = 0$ on a metallic boundary and $g(x, y) = 0$ on a magnetic boundary, where $\boldsymbol{n}$ is normal to the boundary. We therefore find in region 1 ($w/2 \leqslant |x| \leqslant s/2, t_1 \leqslant y \leqslant b$) that

$$g_1(x, y) = \sum_{n=0}^{\infty} \eta_{1n} \cos k_{x1n}\left(x - \frac{w}{2}\right) \cos \frac{n\pi}{t_1'}(y - t_1) \quad (6)$$

where

$$k_{x1n} = \begin{cases} \sqrt{k_c^2 - \left(\dfrac{n\pi}{t_1'}\right)^2} & k_c \geqslant \dfrac{n\pi}{t_1'} \quad (7a) \\ -j\sqrt{\left(\dfrac{n\pi}{t_1'}\right)^2 - k_c^2} & k_c \leqslant \dfrac{n\pi}{t_1'}. \quad (7b) \end{cases}$$

In region 2 ($0 \leqslant |x| \leqslant s/2, 0 \leqslant y \leqslant t$), we find that

$$g_2(x, y) = \sum_{m=0}^{\infty} \eta_{2m} \sin k_{x2m} x \cos \frac{m\pi}{t}(y - t). \quad (8)$$

In region 3 ($s/2 \leqslant |x| \leqslant a_1, 0 \leqslant y \leqslant b$), we find that

$$g_3(x, y) = \sum_{p=0}^{\infty} \eta_{3p} \cos k_{x3p}(x - a_1) \cos \frac{p\pi}{b}(y - b) \quad (9)$$

where k_{x2m} and k_{x3p} are defined similarly to k_{x1n}. Substituting (6), (8), and (9) into (5a) and performing the operations, we then find the transverse electric fields in the three regions as

$$\boldsymbol{e}_1(x, y) = \sum_{n=0}^{\infty} \eta_{1n} \left[\frac{n\pi}{t_1'} \cos k_{x1n}\left(x - \frac{w}{2}\right) \sin \frac{n\pi}{t_1'}(y - t_1)\boldsymbol{a}_x - k_{x1n} \sin k_{x1n}\left(x - \frac{w}{2}\right) \cos \frac{n\pi}{t_1'}(y - t_1)\boldsymbol{a}_y \right] \quad (10a)$$

$$\boldsymbol{e}_2(x, y) = \sum_{m=0}^{\infty} \eta_{2m} \left[\frac{m\pi}{t} \sin k_{x2m} x \sin \frac{m\pi}{t}(y - t)\boldsymbol{a}_x + k_{x2m} \cos k_{x2m} x \cos \frac{m\pi}{t}(y - t)\boldsymbol{a}_y \right] \quad (10b)$$

and

$$\boldsymbol{e}_3(x, y) = \sum_{p=0}^{\infty} \eta_{3p} \left[\frac{p\pi}{b} \cos k_{x3p}(x - a_1) \sin \frac{p\pi}{b}(y - b)\boldsymbol{a}_x - k_{x3p} \sin k_{x3p}(x - a_1) \cos \frac{p\pi}{b}(y - b)\boldsymbol{a}_y \right]. \quad (10c)$$

At $x = s/2$, the BC's require that the tangential electric and magnetic fields be continuous. Additionally, the tangential electric fields should vanish on the conducting walls of the septum. Applying these conditions, we obtain the following expressions for the coefficients η_{1n}, η_{2m}, and η_{3p}:

$$\eta_{1n} = \frac{-1}{\epsilon_n t' k_{x1n} \sin k_{x1n} d} \int_{t_1}^{b} E\,\mathrm{gap}_1(y) \cos \frac{n\pi}{t_1'}(y - t_1)\, dy \quad (11a)$$

$$\eta_{2m} = \frac{1}{\epsilon_m t k_{x2m} \cos k_{x2m} \dfrac{s}{2}} \int_{0}^{t} E\,\mathrm{gap}_2(y) \cos \frac{m\pi}{t}(y - t)\, dy \quad (11b)$$

$$\eta_{3p} = \frac{1}{\epsilon_p b k_{x3p} \sin k_{x3p} h} \left\{ \int_{t_1}^{b} E\,\mathrm{gap}_1(y) \cos \frac{p\pi}{b}(y - b)\, dy + \int_{0}^{t} E\,\mathrm{gap}_2(y) \cos \frac{p\pi}{b}(y - b)\, dy \right\} \quad (11c)$$

where

$$\epsilon_i = \begin{cases} 1 & i = 0 \\ 1/2 & i \neq 0. \end{cases}$$

The continuity of (6), (8), and (9) at the junctions between regions yield the following integral equations:

$$\sum_{n=0}^{\infty} \frac{-\cot k_{x1n} d}{\epsilon_n t_1' k_{x1n}} \cos \frac{n\pi}{t_1'}(y - t_1) \int_{t_1}^{b} E\,\mathrm{gap}_1 \cos \frac{n\pi}{t_1'}(y - t_1)\, dy = \sum_{p=0}^{\infty} \frac{\cot k_{x3p} h}{\epsilon_p b k_{x3p}} \cos \frac{p\pi}{b}(y - b) \left\{ \int_{t_1}^{b} E\,\mathrm{gap}_1(y) \cos \frac{p\pi}{b}(y - b)\, dy + \int_{0}^{t} E\,\mathrm{gap}_2(y) \cos \frac{p\pi}{b}(y - b)\, dy \right\} \quad (12a)$$

at the junction of regions 1 and 3, and

$$\sum_{m=0}^{\infty} \frac{\tan k_{x2m} s/2}{\epsilon_m t k_{x2m}} \cos \frac{m\pi}{t}(y - t) \int_{0}^{t} E\,\mathrm{gap}_2(y) \cos \frac{m\pi}{t}(y - t)\, dy = \sum_{p=0}^{\infty} \frac{\cot k_{x3p} h}{\epsilon_p b k_{x3p}} \cos \frac{p\pi}{b}(y - b) \left\{ \int_{t_1}^{b} E\,\mathrm{gap}_1(y) \cos \frac{p\pi}{b}(y - b)\, dy + \int_{0}^{t} E\,\mathrm{gap}_2(y) \cos \frac{p\pi}{b}(y - b)\, dy \right\} \quad (12b)$$

at the junction of regions 2 and 3. Note that we have assumed w'/b to be very small or approaching zero in matching the electric fields. In our experimental model, we used $w'/b = 0.05$, but we have not tested larger values of w'/b.

Equation (12) is an integral eigenvalue problem. An exact analytical solution to the equation is not possible. However, a numerical solution may be obtained by the application of the Ritz–Galerkin method.

III. Formulation of Matrix Eigenvalue Problem and Its Numerical Solution

Recently, the Ritz–Galerkin technique was applied to the analysis of double ridged waveguide [6], [11], [14]. This technique consists of expanding the unknown functions in terms of suitable known functions, and then requiring that the resultant equations be orthogonal to each expansion function. A matrix equation thus obtained may subsequently be solved by matrix theory. In the present case, the solution is complicated by the fact that we have two junction regions in the same cross-sectional plane.

Proceeding with the solution, (10) leads us to expand the unknown junction fields in the eigenfunctions of regions 1 and 2 as

$$E\,\mathrm{gap}_1(y) = \sum_{j=0}^{J} A_j \cos\frac{j\pi}{t_1'}(y - t_1) \tag{13a}$$

and

$$E\,\mathrm{gap}_2(y) = \sum_{j=0}^{J} B_j \cos\frac{j\pi}{t}(y - t). \tag{13b}$$

Substituting (13) into (12) and taking the inner products of the resultant equations with $\cos\frac{q\pi}{t_1'}(y - t_1)$ and $\cos\frac{q\pi}{t}(y - t)$, respectively, as suggested by the Ritz–Galerkin method, we obtain the following equations:

$$\sum_{j=0}^{J}\left[\frac{\cot k_{x1q}d}{k_{x1q}}\epsilon_q t_1'\delta(q-j) + \sum_{p=0}^{L} T_p P_{1jp} P_{1qp}\right] A_j + \sum_{j=0}^{J}\left[\sum_{p=0}^{L} T_p P_{1qp} P_{2jp}\right] B_j = 0 \tag{14a}$$

$$\sum_{j=0}^{J}\left[\sum_{p=0}^{L} T_p P_{1jp} P_{2qp}\right] A_j + \sum_{j=0}^{J}\left[\frac{-\tan k_{x2q}s/2}{k_{x2q}}\epsilon_q t\delta(q-j) + \sum_{p=0}^{L} T_p P_{2jp} P_{2qp}\right] B_j = 0 \tag{14b}$$

for $q = 0,1,2,\cdots,J$, and where

$$T_p = \frac{\cot k_{x3p}h}{\epsilon_p b k_{x3p}} \tag{15}$$

$$P_{1jp} = \int_{t_1}^{b} \cos\frac{j\pi}{t_1'}(y - t_1')\cos\frac{p\pi}{b}(y - b)\,dy \tag{16}$$

$$P_{2jp} = \int_{0}^{t} \cos\frac{j\pi}{t}(y - t)\cos\frac{p\pi}{b}(y - b)\,dy. \tag{17}$$

The infinite summations have been truncated to $(J+1)$ terms in regions 1 and 2 and $(L+1)$ terms in region 3. Equation (14) may be expressed in matrix form as

$$[H_A(k_c)\,|\,H_B(k_c)]\begin{bmatrix} A \\ \hline B \end{bmatrix} = [0] \tag{18}$$

where the $H_A(k_c)$ matrix elements are the coefficients of the unknown vector A, and the $H_B(k_c)$ elements are the coefficients of vector B, where

$$[A] = [A_1, A_2, \cdots, A_J]^T \tag{19}$$

$$[B] = [B_1, B_2, \cdots, B_J]^T. \tag{20}$$

Equation (18) is a general matrix eigenvalue problem. The eigenvalues are solutions of the nonlinear equation

$$\det|H_A(k_c)\,|\,H_B(k_c)| = 0. \tag{21}$$

The smallest eigenvalue corresponds to the largest cutoff wavelength of the TE_{10} mode. The vector $[A|B]$, which is the solution of (18) for a particular k_c, is the associated eigenvector, which is related to the coefficients η_{1n}, η_{2m}, and η_{3p} by

$$\eta_{1n} = \frac{-A_n}{k_{x1n}\sin k_{x1n}d} \tag{22a}$$

$$\eta_{2m} = \frac{B_m}{k_{x2m}\cos k_{x2m}s/2} \tag{22b}$$

$$\eta_{3p} = \frac{1}{\epsilon_p b k_{x3p}\sin k_{x3p}h}\sum_{j=0}^{J}\left(A_j P_{1jp} + B_j P_{2jp}\right). \tag{22c}$$

The nonlinear equation (21) may be solved by applying a solution developed by Barlow and Jones [12]. The associated dominant eigenvectors may be determined by the application of a technique obtained by Montgomery [11]. This method makes each element of the solution vector arbitrary successively and calculates the error norm of each solution vector. By choosing the solution vector with the smallest norm, the dominant eigenvector is determined. Fig. 2 illustrates a typical eigenvalue spectrum. Mathematical singularities of (21) should be carefully avoided in solving (21) to obtain the eigenvalues.

IV. Numerical Results

In order to check the correctness of the analysis, single-ridged waveguides of various geometries were analyzed, for which case $w = s$; i.e., the septum becomes a solid ridge. Rapid convergence was observed when J and L were increased. For $J \geqslant 12$ and $L \geqslant 15$, the calculation is precise to the third digit after the decimal point. A comparison of the present results with those from Hopfer [2] is illustrated in Table I. The data illustrate that the method yields good agreement with the known results for the single-ridged guide. The impedance comparison is also given in Table I,

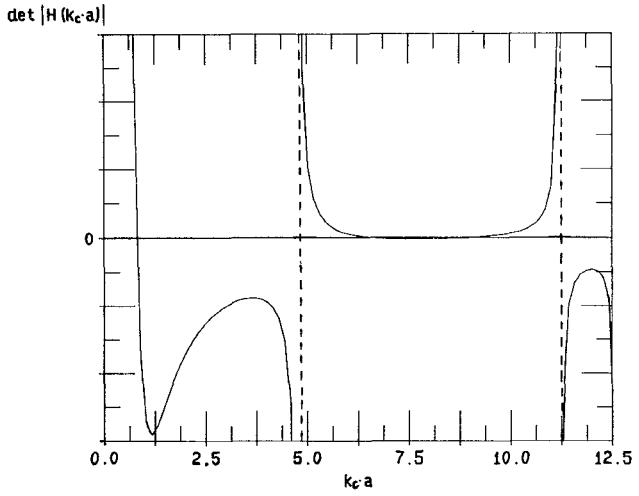

Fig. 2. Plot of typical eigenvalue equation.

TABLE I
COMPARISON WITH OTHER THEORY

$\frac{t}{b}$	Hopfer [2]			Present		
	λ_{c10}/a	$\lambda_{c10}/\lambda_{c20}$	Z_∞	λ_{c10}/a	$\lambda_{c10}/\lambda_{c20}$	Z_∞
0.10	4.643	5.09	69.93	4.6278	5.1434	70.033
0.15	4.072	4.42	90.91	4.0606	4.5136	90.586
0.20	3.701	3.94	108.69	3.7137	4.1286	107.828
0.25	3.425	3.63	128.21	3.4179	3.8078	126.695
0.30	3.206	3.38	144.93	3.1984	3.5607	143.995
0.35	3.023	3.14	161.29	3.0148	3.3616	161.280

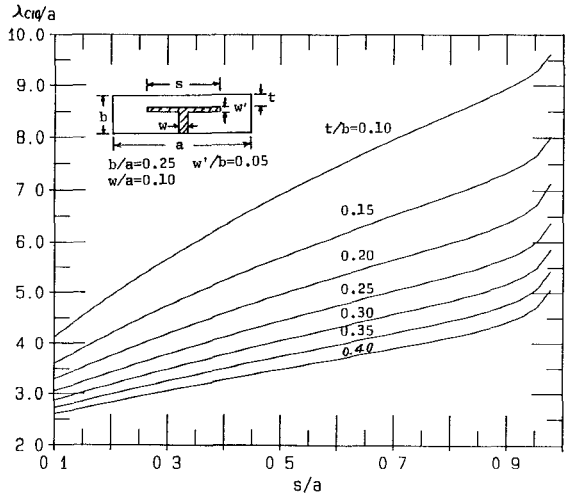

Fig. 3. Variation of normalized cutoff wavelength (λ_{c10}/a) of dominant TE_{10} mode with gap width ratio (s/a).

which will be explained in Section V. All the subsequent computations were carried out with $J=12$ and $L=15$.

In Figs. 3 and 4, the normalized cutoff wavelengths λ_{cn0}/a of the TE_{10} and TE_{20} modes are plotted as a function of s/a, with t/b as a parameter. Fig. 5 shows the bandwidth characteristics of the STSG. The aspect ratio b/a for these curves is fixed at 0.25. Figs. 6–8 gives

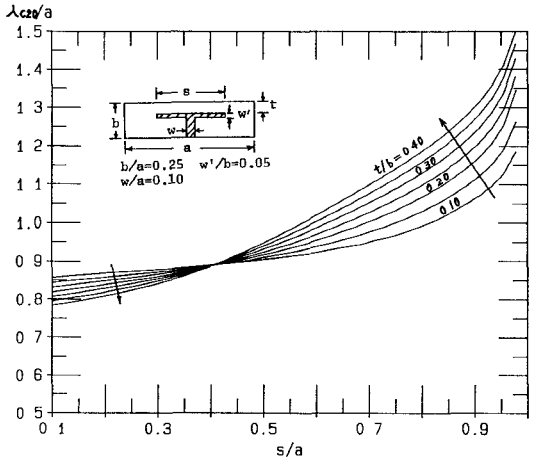

Fig. 4. Variation of normalized cutoff wavelength (λ_{c20}/a) of TE_{20} mode with gap width ratio (s/a).

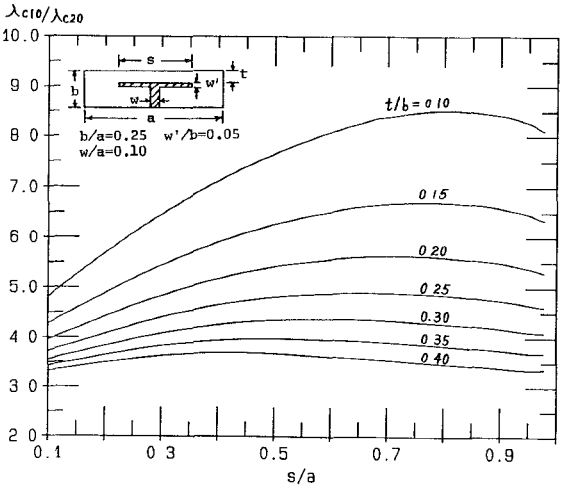

Fig. 5. Variation of bandwidth ($\lambda_{c10}/\lambda_{c20}$) characteristics with gap width ratio (s/a).

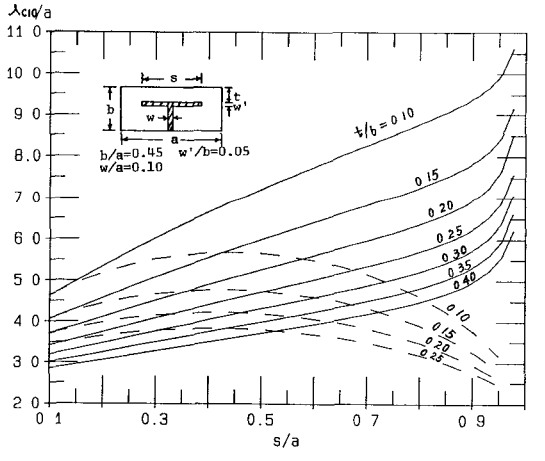

Fig. 6. Variation of normalized cutoff wavelength (λ_{c10}/a) of dominant TE_{10} mode with gap width ratio (s/a). Solid lines: single T-septum guide; dashed lines: single ridged guide of the same geometry with a solid ridge ($w=s$).

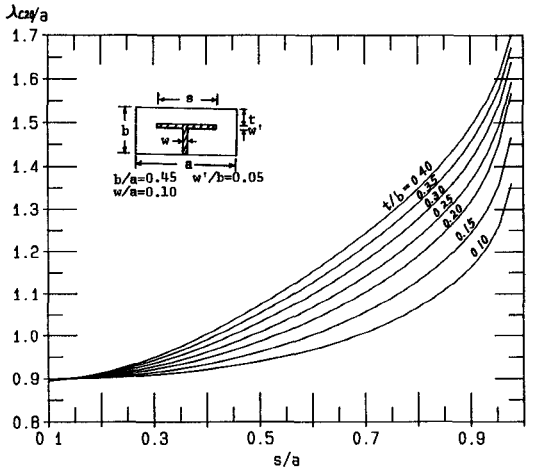

Fig. 7. Variation of normalized cutoff wavelength (λ_{c20}/a) of TE_{20} mode with gap width ratio (s/a).

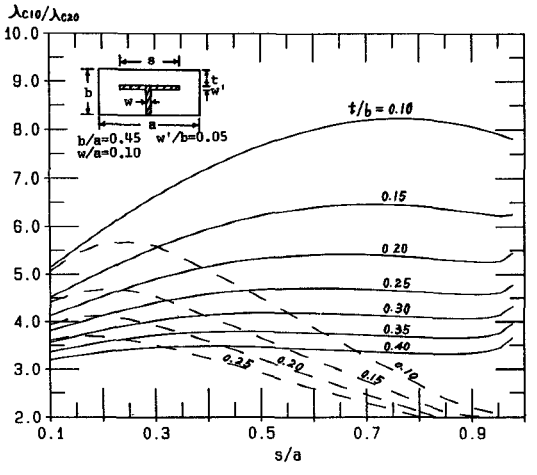

Fig. 8. Variation of bandwidth ($\lambda_{c10}/\lambda_{c20}$) characteristics with gap width ratio (s/a). Solid lines: single T-septum guide; dashed lines: single ridged guide of the same geometry with a solid ridge ($w = s$).

another set of data for $b/a = 0.45$. Also superposed as dashed lines in Figs. 6 and 8 are the corresponding properties of SRG[2] with identical t/b and s/a, subject to the error in reproducing the curves. These curves are directly applicable to a double T-septum guide cross section of identical s/a and t/b ratios, but of an aspect ratio b/a which is twice that of the DTSG. Note that the cutoff wavelength increases monotonically with s/a for fixed t/b, and is always greater than that for SRG. The bandwidth (Fig. 8) of the STSG is much greater than that of the SRG when s/a is greater than 0.2, and reaches a peak around $s/a = 0.7$. The bandwidth of the STSG can be made even wider if optimum parameters are chosen.

V. T-Septum Waveguide Characteristic Impedance

To design a transition between the T-septum waveguide and a coaxial line or between two dissimilar waveguides, the impedance of the waveguide is needed. Usually, the impedance definition from power considerations is desired, i.e.,

$$Z = \frac{V_0^2}{2P_0} \tag{23}$$

where P_0 is the average power carried by the guide, and V_0 is the peak voltage across the center of the septum, which can be expressed as

$$V_0 = \int_0^t e_y(x=0, y)\, dy. \tag{24}$$

Employing (10b) and (22b), we find that

$$V_0 = B_0 \frac{t}{\cos k_c s/2}. \tag{25}$$

The average power is given by

$$P_0 = \frac{1}{2Z_h} \iint_S |e_t|^2\, dx\, dy \tag{26}$$

where S is the cross section of the guide. Recalling (10), we can express (26) as

$$P_0 = \frac{1}{Z_h}[I_1 + I_2 + I_3] \tag{27}$$

where

$$I_1 = \sum_{n=0}^{\infty} \frac{1}{4}\eta_{1n}^2 \cdot \left[(n\pi)^2 \frac{d}{t_1'}\left(1 + \frac{\sin 2k_{x1n}d}{2k_{x1n}d}\right) + 2\epsilon_n k_{x1n}^2 t_1' d\left(1 - \frac{\sin 2k_{x1n}d}{2k_{x1n}d}\right)\right] \tag{28a}$$

$$I_2 = \sum_{m=0}^{\infty} \frac{1}{8}\eta_{2m}^2 \cdot \left[(m\pi)^2 \frac{s}{t}\left(1 - \frac{\sin k_{x2m}s}{k_{x2m}s}\right) + 2\epsilon_m k_{x2m}^2 ts\left(1 + \frac{\sin k_{x2m}s}{k_{x2m}s}\right)\right] \tag{28b}$$

and

$$I_3 = \sum_{p=0}^{\infty} \frac{1}{4}\eta_3^2 \cdot \left[(p\pi)^2 \frac{h}{b}\left(1 + \frac{\sin 2k_{x3p}h}{2k_{x3p}h}\right) + 2\epsilon_p k_{x3p}^2 bh\left(1 - \frac{\sin 2k_{x3p}h}{2k_{x3p}h}\right)\right]. \tag{28c}$$

Hence

$$Z = \frac{Z_\infty}{\sqrt{1 + (\lambda/\lambda_c)^2}} \tag{29}$$

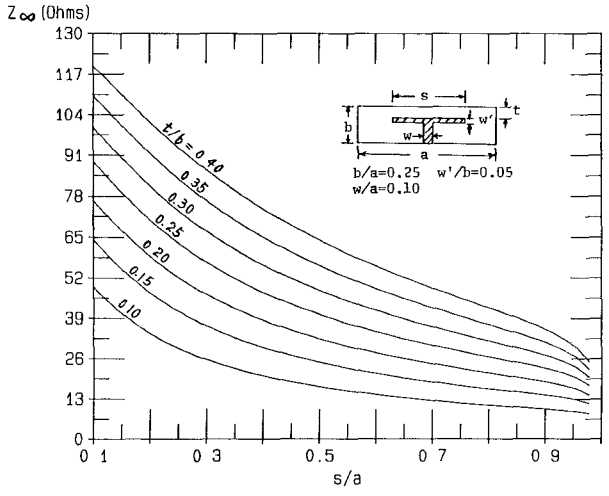

Fig. 9. Characteristic impedance at infinite frequency versus gap width ratio (s/a) with $b/a = 0.25$.

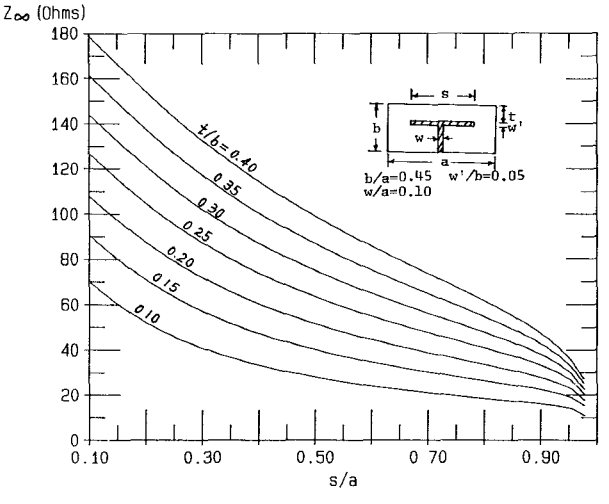

Fig. 10. Characteristic impedance at infinite frequency versus gap width ratio (s/a) with $b/a = 0.45$.

where Z_∞ is the characteristic impedance at infinite frequency:

$$Z_\infty = \sqrt{\frac{\mu}{\epsilon}} \frac{B_0^2 t^2}{2(I_1 + I_2 + I_3)\cos^2 k_c s/2}. \qquad (30)$$

The correctness of the impedance equation was confirmed by calculations on the SRG as shown in Table I. A difference of less than 1 percent was observed.

Figs. 9 and 10 illustrate the impedance quantity Z_∞ for aspect ratios $b/a = 0.25$ and 0.45, respectively. For fixed t/b, the impedance decreases monotonically with increasing s/a. On the other hand, for fixed s/a, Z_∞ increases with t/b. Compared with that of SRG, Z_∞ does not change dramatically.

The characteristic impedance curves may also be applied to DTSG, but their values must be doubled, and the aspect ratio b/a has to be treated as in the case of the cutoff wavelength.

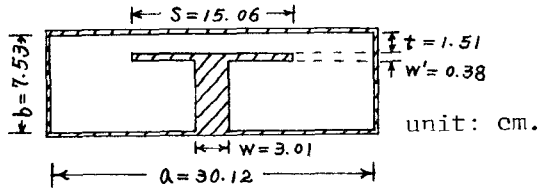

Fig. 11. The cross section of the experimental STSG.

TABLE II
COMPARISON OF CALCULATED AND MEASURED RESULTS

Parameters	Calculated	Measured	Error
Cutoff of TE_{10} mode (MHz)	200	216	8%
Cutoff of TE_{20} mode (MHz)	1085	1092	0.65%
Bandwidth	5 43	5.06	6 7%
Characteristic impedance $Z_\infty(\Omega)$	32.5	36.02	10.8%

VI. Experimental Verification

A single T-septum waveguide having the cross-sectional dimensions shown in Fig. 11 has been tested. The waveguide parameters are $b/a = 0.25$, $t/b = 0.20$, $s/a = 0.50$, $w'/b = 0.05$, and $w/a = 0.10$. The electrical parameters of the waveguide were measured on a Hewlett Packard model 8754A Network Analyzer. The cutoff frequency of the TE_{10} mode was determined by measuring the frequency at the point where the insertion loss dropped to -3 dB, and the cutoff of the TE_{20} mode was found by forming the waveguide as a resonant cavity and measuring the resonant frequency of the mode corresponding to the TE_{20}. The waveguide cavity had the cross-sectional dimensions shown in Fig. 11. Using the network analyzer, the swept-frequency display of insertion loss versus frequency showed that the next resonant dip above the TE_{10} mode occurred at the predicted frequency of the TE_{20} mode. The characteristic impedance of the waveguide was determined by the method described in [15]. Using this method, one measures the normalized input impedance which traces a circle on the Smith chart as frequency is varied. The center of the circle has a real component equal to the normalized characteristic impedance of the waveguide.

A comparison of the calculated parameters and the measured results is given in Table II. The calculated data are from Figs. 3–5 and 9. The error column signifies the agreement between the calculated and the measured values of each parameter. The experimental results checked with the T-septum waveguide calculated cutoffs to within a few percent. The calculated and measured characteristics impedances agree to within 10.8 percent. A tapered length of stripline was used to connect the waveguide to the 50-Ω coaxial line. This connection would affect the impedance measurement to some extent, and might account for the error obtained.

VII. Discussion

The T-septum waveguide has been analyzed to develop appropriate equations and curves for design. The design curves show that the cutoff wavelength of the dominant

TE_{10} mode for these guides is much greater, when $s/a > 0.3$, than that of the conventional ridged guides with the same geometries. The bandwidth of the guide keeps increasing when $s/a > 0.3$, and is much greater than that of the SRG. For example, the STSG shown in Fig. 6 with $t/b = 0.10$ and $s/a = 0.70$ would have a cutoff wavelength of $8.290a$ and a bandwidth ($\lambda_{c10}/\lambda_{c20}$) of 8.203, while the SRG of the same geometry has a cutoff wavelength of $5.157a$ and a bandwidth of 3.25. An improvement of 1.6 times that of the SRG has been achieved for the cutoff wavelength, and 2.5 times that of the SRG for the bandwidth. Note that the bandwidth curves are different from those suggested in [7] and [8], in which the correct second lowest eigenvalues were not taken into account. The characteristic impedance of the guides has been compared with that of the SRG, and no dramatic change was found.

The agreement between the calculated results and the measured values is within about 10 percent, as shown in Table II. We expect that the percent error would be reduced by more extensive measurements on waveguides having a wide range of dimensions. For most engineering applications, the curves and equations presented should be quite adequate.

Further studies are in progress, which include determination of the attenuation in the guides and their power-handling capabilities.

REFERENCES

[1] S. B. Cohn, "Properties of ridged wave guide," *Proc. IRE*, vol. 35, pp. 783–788, Aug. 1947.

[2] S. Hopfer, "The design of ridged waveguides," *IRE Trans. Microwave Theory Tech.*, vol. MTT-3, pp. 20–29, Oct. 1955.

[3] J. R. Pyle, "The cutoff wavelength of the TE_{10} mode in ridged rectangular waveguide of any aspect ratio," *IEEE Trans. Microwave Theory Tech.*, vol. MTT-14, pp. 175–183, Apr. 1966.

[4] W. J. Getsinger, "Ridged waveguide field description and application to directional couplers," *IRE Trans. Microwave Theory Tech.*, vol. MTT-10, pp. 41–50, Jan. 1962.

[5] G. Magerl, "Ridged waveguide with inhomogeneous dielectric slab loading," *IEEE Trans. Microwave Theory Tech.*, vol. MTT-26, pp. 413–416, June 1978.

[6] D. Dasgupta and P. K. Saha, "Rectangular waveguide with two double ridges," *IEEE Trans. Microwave Theory Tech.*, vol. MTT-31, pp. 938–941, Nov. 1983.

[7] G. G. Mazumder and P. K. Saha, "A novel rectangular waveguide with double T-septums," *IEEE Trans. Microwave Theory Tech.*, vol. MTT-33, pp. 1235–1238, Nov. 1985.

[8] G. G. Mazumder and P. K. Saha, "Rectangular waveguide with T-shaped septa," *IEEE Trans. Microwave Theory Tech.*, pp. 201–204, Feb. 1987.

[9] F. B. Hildebrand, *Methods of Applied Mathematics*. Englewood Cliffs, NJ: Prentice-Hall, 1965, pp. 279–286.

[10] R. F. Harrington, *Field Computation by Moment Method*. New York: Macmillan, 1968.

[11] J. P. Montgomery, "On the complete eigenvalue solution of ridged waveguide," *IEEE Trans. Microwave Theory Tech.*, vol. MTT-19, pp. 547–555, June 1971.

[12] C. A. Barlow, Jr., and E. L. Jones, "A method for the solution of roots of a nonlinear equation and for solution of the general eigenvalue problem," *J. Ass. Comput. Mach.*, vol. 13, pp. 135–142, Jan. 1966.

[13] R. E. Collin, *Field Theory of Guided Waves*. New York, McGraw-Hill, 1960.

[14] D. Dasgupta and P. K. Saha, "Eigenvalue spectrum of rectangular waveguide with two symmetrically placed double ridges," *IEEE Trans. Microwave Theory. Tech.*, vol. MTT-29, pp. 47–51, Jan. 1981.

[15] W. T. Joines, "The characteristic impedance of symmetrical strip transmission lines with undesired modes suppressed," Ph.D. dissertation, Duke University, 1964.

Yang Zhang was born in Shenyang, China, on December 5, 1957. He received the B.S.E.E. degree with high honors from Chengdu Institute of Radio Engineering, Chengdu, China, in 1982, and the M.S. degree in electrical engineering from Duke University, Durham, NC, in 1984.

He is presently with the Department of Electrical Engineering, Duke University, as a Research Assistant, where he is working towards the Ph.D. degree in microwave engineering. His research interests are in the area of electromagnetic wave interactions with materials, with applications to transmission lines, antennas, and microwave-induced hyperthermia.

Mr. Zhang is a member of Eta Kappa Nu.

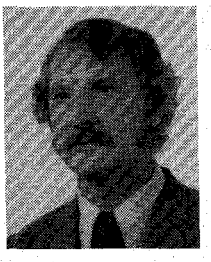

William T. Joines (M'61) was born in Granite Falls, NC, on November 20, 1931. He received the B.S.E.E. degree with high honors from North Carolina State University, Raleigh, in 1959, and the M.S. and Ph.D. degrees in electrical engineering from Duke University, Durham, NC, in 1961 and 1964, respectively.

From 1959 to 1966, he was a member of the Technical Staff at Bell Laboratories, Winston-Salem, NC, where he was engaged in research and development of microwave components and systems for military applications. He joined the faculty of Duke University in 1966, and is currently a Professor of Electrical Engineering. His research and teaching interests are in the area of electromagnetic wave interactions with materials.